FIV2024
IGUAÇU FALLS, BRAZIL
2-5 JULY 2024

FIV2024: FSI² & FIV + N
10th International Symposium on Fluid-Structure Interactions,
Flow-Sound Interactions, Flow-Induced Vibration & Noise

# FIV2024-0126
# BENDING-AXIAL-TORSIONAL DYNAMICS OF PIPES CONVEYING FLUID

**Vitor Schwenck Franco Maciel**
**Guilherme Vernizzi**
Offshore Mechanics Laboratory, Escola Politécnica, University of São Paulo, Brazil
vitor.maciel@usp.br
guilherme.jorge.lopes@usp.br

**Mojtaba Kheiri**
Fluid-Structure Interactions & Aeroelasticity Laboratory, Concordia University, Canada
mojtaba.kheiri@concordia.ca

**Guilherme Rosa Franzini**
Offshore Mechanics Laboratory, Escola Politécnica, University of São Paulo, Brazil
gfranzini@usp.br

***Abstract.*** *The present work aims at characterizing the effects of including torsion when modeling pipes conveying fluid. A three-dimensional nonlinear model for the dynamics of a cantilevered pipe discharging fluid is presented. Besides the consideration of an extensible centreline for the pipe, the occurrence of torsional displacements is also taken into account. As a preliminary investigation of the effects of torsion on the stability and dynamics of the pipe, a torsional moment is applied at its free end. The dynamics is formulated around the axial and torsional static configurations which are evaluated numerically while considering the nonlinear couplings terms. The equations are discretized using Galerkin's method and nonlinearities up to the cubic order are considered in the mathematical model. By comparing the stability conditions of systems with and without the applied torsional moment, it is shown that this addition strictly reduces the critical flow velocities. Depending on the parameters of the system, flutter and divergence may occur, and scenarios in which the presence of internal flow re-stabilizes the system are also presented. By numerically integrating the equations of motion, it is shown that the presence of the torsional moment may induce three-dimensional motions even when two-dimensional initial conditions are given.*

***Keywords:*** *Pipes conveying fluid, Linear dynamics, Nonlinear dynamics.*

## 1. INTRODUCTION

Systems of pipes conveying fluid subject to internal-axial-flow-induced vibrations have been established decades ago as a new model dynamical problem (Païdoussis and Li (1992), Païdoussis (2022)). Practical applications involving such systems can be found in heat exchangers, offshore risers and, more recently, the injection and storing of carbon dioxide within underground or submarine caverns. Moreover, from an academic point of view, pipes conveying fluid are capable of displaying a wide array of rich and even unexpected dynamical behavior, in both linear and nonlinear analyses. Consequently, a rapidly increasing amount of academic interest has been put in studying this particular type of fluid-structure interaction. In the past decades, the published mathematical models on the topic have become increasingly more complex. Generally, this evolution is characterized by the use of more complex flow models or more complex structural models for the pipe. The works herein mentioned comprise what are considered as the main advancements in the latter aspect of said mathematical models.

The two-dimensional (2-D) dynamics and stability of a discrete system composed of articulated rigid pipes was studied in (Benjamin, 1961). Among its many contributions, the derivation of a modified version of the Hamilton's principle capable of including this *open* system is of note (i.e. one across which mass and momentum are transported). The reader interested in further discussions regarding appropriate variational principles for *open* systems is referred to (McIver, 1973), (Irschik and Holl, 2002), (Casetta and Pesce, 2013) and, for the specific case of pipes conveying fluid, (Kheiri and Païdoussis, 2014). Gregory and Païdoussis (1966a) extended Benjamin's work by presenting a linear 2-D model for a continuous and inextensible pipe in the absence of gravitational effects. The inclusion of gravity was made in (Païdoussis, 1970), where it was discussed that a hanging discharging pipe can only lose stability via a Hopf bifurcation (flutter), similarly as the horizontal one. However, standing discharging pipes were shown to display richer dynamical

features. Among these, the fact that a pipe which had undergone divergence due to its own weight could be re-stabilized by increasing the internal flow velocity is mentioned. Yet more, further increase in the flow velocity led to the more usual dynamic instability due to a Hopf bifurcation.

The limit-cycle oscillations experienced by pipes conveying fluid at a post-critical flow velocity had been experimentally observed for decades (e.g. in Gregory and Païdoussis (1966b)). The desire to obtain this behavior from mathematical models motivated the inclusion of geometrical nonlinearities in subsequent publications. The authors in (Semler *et al.*, 1992) carried out a systematic comparison between existing nonlinear formulations and presented their own set of nonlinear equations for the 2-D motions of inextensible pipes conveying fluid. An additional development was made in (Wadham-Gagnon *et al.*, 2006), where the equations presented in (Semler *et al.*, 1992) were extended to three dimensions. It was shown that the motions of the pipe could be 2-D or 3-D depending on the parameters characterizing the pipe and internal flow velocity.

Another category of improvements is comprised of considering the centreline of the pipe as being extensible. In (Ghayesh *et al.*, 2013), the 2-D dynamics and stability of extensible pipes were studied and, amidst other conclusions, it was shown that extensible pipes can require larger flow velocities to undergo flutter. These additional complexities in modeling pipes were both considered in (Askarian and Kheiri, 2018), where a 3-D mathematical model for an extensible pipe was presented. Generally, in both these references addressing extensible pipes, the qualitative aspects of the dynamics of the system were shown to be fundamentally similar to inextensible pipes. An extensive review of studies published before 2014 can be found in (Païdoussis, 2014).

The main purpose of the present work is to further contribute to the ever growing complexity of mathematical models for pipes conveying fluid. To the best of the authors' knowledge, the role of torsion in the dynamics and stability of pipes conveying fluid has not yet been studied. Besides the inclusion of extensibility, the 3-D mathematical model herein presented also includes the torsional degree-of-freedom (DOF) in the structural model of the pipe. This is made similarly as was made in (Crespo da Silva, 1988). The paper is organized as follows: in Sec. 2, the mathematical model is described and the equations of motion, presented. Then, Sec. 3 presents the main methodological aspects with which the results presented in Sec. 4 are obtained. Finally, Sec. 5 gathers the main conclusions drawn.

## 2. MATHEMATICAL MODEL

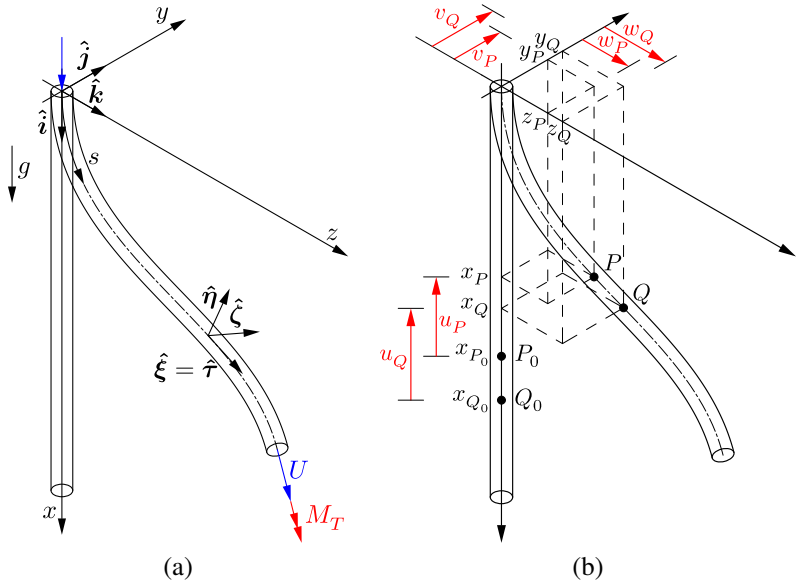


Figure 1. Sketches of the hanging cantilevered pipe showing the (a) global $(\hat{\boldsymbol{i}}, \hat{\boldsymbol{j}}, \hat{\boldsymbol{k}})$ and local $(\hat{\boldsymbol{\xi}}, \hat{\boldsymbol{\eta}}, \hat{\boldsymbol{\zeta}})$ reference frames and (b) definition of the transverse and axial displacements.

Consider the system composed of a hanging cantilevered pipe discharging fluid shown in Fig. 1(a). The pipe has length $L$, mass per unit length $m$, Young's modulus $E$ and shear modulus $G$. The conveyed fluid has mass per unit length $M$ and flows at a constant velocity $U$, relative to the pipe. While $(\hat{\boldsymbol{i}}, \hat{\boldsymbol{j}}, \hat{\boldsymbol{k}})$ is a global fixed coordinate system, $(\hat{\boldsymbol{\xi}}, \hat{\boldsymbol{\eta}}, \hat{\boldsymbol{\zeta}})$ is a local reference frame. A curvilinear coordinate $s$ is defined along the length of the pipe (see Fig. 1(a)).

The moments of inertia of the cross section with respect to the $y$- and $z$-axes are denoted by $I_y$ and $I_z$, respectively, while $I_p$ is the polar moment of inertia. Finally, the fourth-order polar moment of the cross sections is denoted by $I_4$. The pipe is straight in its undeflected configuration and the gravitational acceleration is denoted by $\boldsymbol{g} = g\hat{\boldsymbol{i}}$.

A linear-elastic constitutive behavior is considered for the pipe material and its properties ($E$, $G$ and $m$) are assumed

to be constant along its length. The plug-flow model is used: the fluid is considered as incompressible and its velocity profile inside the pipe, as uniform. The pipe is assumed to behave as a Kirchhoff beam and, since the cross sections are expected to be thin-walled, no warping is considered. Accordingly, the cross sections are assumed to behave as rigid bodies and, in addition, their rotary inertia is neglected. While large displacements are considered (nonlinearities up to $\mathcal{O}(\varepsilon^3)$ in the equations of motion), the strains are assumed to be small given the constitutive behavior expected for the pipe material. Allowing for a preliminary investigation of the role of torsion in the dynamics and stability of the pipe, a torsional moment of magnitude $M_T$ is applied at its free end. The equations of motion are obtained using the generalized Hamilton's principle for nonmaterial volumes published in (Casetta and Pesce, 2013).

### 2.1 Kinematic description - displacements and rotations

The transverse and axial displacements used are defined in Fig. 1(b). The Euler angles used to characterize rotations, on the other hand, are defined as follows: firstly, a rotation $\theta_y$ is given around the $y$-axis, leading to the $(\xi_1, \eta_1, \zeta_1)$ coordinate system (see Fig. 2(a)); secondly, a rotation $\theta_z$ is given around the $\zeta_1$-axis, leading to the $(\xi_2, \eta_2, \zeta_2)$ coordinate system (see Fig. 2(b)); lastly, a rotation $\theta_x$ around the $\xi_2$-axis leads to the $(\xi, \eta, \zeta)$ coordinate system (see Fig. 2(c)).

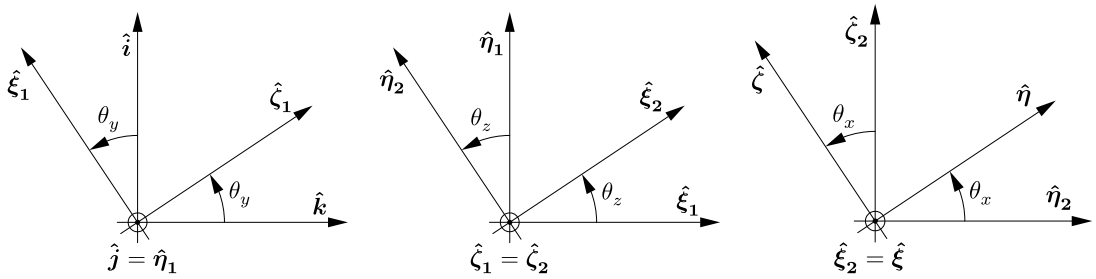


(a) Rotation around the $y$-axis. (b) Rotation around the $\zeta_1$-axis. (c) Rotation around the $\xi_2$-axis.

Figure 2. Definition of the Euler angles.

Therefore, $\theta_x$ is the DOF associated with the torsional displacements and, along with the displacements $u$, $v$ and $w$, allows for a complete kinematic description of a deflected configuration of the pipe. From Figs. 2(a), (b) and (c), direct relations between the $(\hat{\boldsymbol{\imath}}, \hat{\boldsymbol{\jmath}}, \hat{\boldsymbol{k}})$ and $(\hat{\boldsymbol{\xi}}, \hat{\boldsymbol{\eta}}, \hat{\boldsymbol{\zeta}})$ reference frames can be obtained as

$$
\begin{aligned}
&\hat{\boldsymbol{\imath}} = i_\xi \hat{\boldsymbol{\xi}} + i_\eta \hat{\boldsymbol{\eta}} + i_\zeta \hat{\boldsymbol{\zeta}}, \text{ where } \begin{cases} i_\xi = \cos\theta_y \cos\theta_z \\ i_\eta = \sin\theta_y \sin\theta_x - \cos\theta_y \sin\theta_z \cos\theta_x \\ i_\zeta = \sin\theta_y \cos\theta_x + \cos\theta_y \sin\theta_z \sin\theta_x \end{cases}, \\
&\hat{\boldsymbol{\jmath}} = j_\xi \hat{\boldsymbol{\xi}} + j_\eta \hat{\boldsymbol{\eta}} + j_\zeta \hat{\boldsymbol{\zeta}}, \text{ where } \begin{cases} j_\xi = \sin\theta_z \\ j_\eta = \cos\theta_z \cos\theta_x \\ j_\zeta = -\cos\theta_z \sin\theta_x \end{cases}, \text{ and} \\
&\hat{\boldsymbol{k}} = k_\xi \hat{\boldsymbol{\xi}} + k_\eta \hat{\boldsymbol{\eta}} + k_\zeta \hat{\boldsymbol{\zeta}}, \text{ where } \begin{cases} k_\xi = -\sin\theta_y \cos\theta_z \\ k_\eta = \cos\theta_y \sin\theta_x + \sin\theta_y \sin\theta_z \cos\theta_x \\ k_\zeta = \cos\theta_y \cos\theta_x - \sin\theta_y \sin\theta_z \sin\theta_x \end{cases}.
\end{aligned}
\tag{1}
$$

The quadractic strain measure for the centreline of the pipe can be obtained as, using the notation $(\,)' = \partial(\,)/\partial s$,

$$
\varepsilon_q = u' + \frac{v'^2 + w'^2}{2} + \mathcal{O}(\varepsilon^4). \tag{2}
$$

To present the strain measures for a generic material point of the pipe, let $P$ be a point belonging to a cross section at its intersection with the centreline of the pipe. Now let $R$ be a point also contained in that cross section and with coordinates $y_R \hat{\boldsymbol{\eta}} + z_R \hat{\boldsymbol{\zeta}}$ relative to $P$. The Green strain tensor used and the obtained generalized strain measures are

$$
\boldsymbol{E} = \begin{bmatrix} \varepsilon_{\xi\xi} & \varepsilon_{\xi\eta} & \varepsilon_{\xi\zeta} \\ \varepsilon_{\eta\xi} & \varepsilon_{\eta\eta} & \varepsilon_{\eta\zeta} \\ \varepsilon_{\zeta\xi} & \varepsilon_{\zeta\eta} & \varepsilon_{\zeta\zeta} \end{bmatrix}, \; \varepsilon_{\xi\xi} = \frac{\varepsilon^* + C_\xi^2 (z_R^2 + y_R^2)}{2}, \; \varepsilon_{\xi\eta} = -\frac{C_\xi z_R}{2}, \text{ and } \varepsilon_{\xi\zeta} = \frac{C_\xi y_R}{2}, \text{ where} \tag{3}
$$

$$\varepsilon^* = \left(\sqrt{(1+u')^2 + v'^2 + w'^2} - 1\right) + C_\eta z_R - C_\zeta y_R, \text{ and} \tag{4}$$

$$\boldsymbol{C} = C_\xi \hat{\boldsymbol{\xi}} + C_\eta \hat{\boldsymbol{\eta}} + C_\zeta \hat{\boldsymbol{\zeta}}, \text{ where } \begin{cases} C_\xi = \theta_x' + \theta_y' \sin\theta_z \\ C_\eta = \theta_y' \cos\theta_z \cos\theta_x + \theta_z' \sin\theta_x \\ C_\zeta = -\theta_y' \cos\theta_z \sin\theta_x + \theta_z' \cos\theta_x \end{cases} \tag{5}$$

are the generalized nonlinear curvature expressions written in the local $(\hat{\boldsymbol{\xi}}, \hat{\boldsymbol{\eta}}, \hat{\boldsymbol{\zeta}})$ reference frame. Notice that, while $\varepsilon^*$ represents the axial strain which considers the effects of the transverse curvature components $C_\eta$ and $C_\zeta$, $\varepsilon_{\xi\xi}$ also includes the effect of the axial curvature component $C_\xi$, thus including torsional effects. Moreover, due to the assumption that the cross sections move as rigid bodies, $\varepsilon_{\eta\zeta} = \varepsilon_{\zeta\eta} = 0$, as expected. When written in terms of the displacements $u$, $v$, $w$ and $\theta_x$, the expressions for the generalized curvature components become

$$\begin{aligned} C_\xi &= \theta_x' - v'w'' + \mathcal{O}(\varepsilon^4), \\ C_\eta &= -w'' + v''\theta_x + u''w' + w'^2 w'' + \frac{w''v'^2}{2} + \frac{w''\theta_x^2}{2} + u'w'' + \mathcal{O}(\varepsilon^4), \\ C_\zeta &= v'' + w''\theta_x - u'v'' - \frac{v''w'^2}{2} - u''v' - v'^2 v'' - v'w'w'' - \frac{v''\theta_x^2}{2} + \mathcal{O}(\varepsilon^4). \end{aligned} \tag{6}$$

An important observation is that, due to the nonlinearities of $C_\xi$, $\theta_x$ does not provide the direct torsional angles $\theta$ along the length of the pipe. Instead, it is used to compose it along with the transverse displacements $v$ and $w$, i.e., considering terms up to $\mathcal{O}(\varepsilon^3)$,

$$\theta(s) = \int_0^s C_\xi ds = \int_0^s (\theta_x' - v'w'')\, ds. \tag{7}$$

Equation (7) impacts the shape functions used in the discretization of the equations of motion, which is discussed further in Sec. 3. Lastly, the angular velocities used are, using the notation $\dot{(\,)} = \partial(\,)/\partial t$,

$$\boldsymbol{\omega} = \omega_\xi \hat{\boldsymbol{\xi}} + \omega_\eta \hat{\boldsymbol{\eta}} + \omega_\zeta \hat{\boldsymbol{\zeta}}, \text{ where } \begin{cases} \omega_\xi = \dot{\theta}_x + \dot{\theta}_y \sin\theta_z \\ \omega_\eta = \dot{\theta}_y \cos\theta_z \cos\theta_x + \dot{\theta}_z \sin\theta_x \\ \omega_\zeta = -\dot{\theta}_y \cos\theta_z \sin\theta_x + \dot{\theta}_z \cos\theta_x \end{cases}, \tag{8}$$

when written in the local $(\hat{\boldsymbol{\xi}}, \hat{\boldsymbol{\eta}}, \hat{\boldsymbol{\zeta}})$ reference frame. Given that the rotary inertia of the cross sections are assumed to be negligible, the only angular velocity used in the kinetic energy of the pipe is, in terms of $u$, $v$, $w$ and $\theta_x$,

$$\omega_\xi = \dot{\theta}_x - v'\dot{w}' + \mathcal{O}(\varepsilon^4). \tag{9}$$

### 2.2 Dimensionless equations of motion

As mentioned at the beginning of this section, the equations of motion are derived using the generalized Hamilton's principle for nonmaterial volumes. In order to obtain a dimensionless mathematical model, all translational displacements are normalized with respect to the length of the pipe and time is normalized as shown in Eq. (10):

$$\tau = \left(\frac{EI}{m+M}\right)^{1/2} \frac{t}{L^2};\;\; \xi = \frac{u}{L};\;\; \eta = \frac{v}{L};\;\; \zeta = \frac{w}{L}. \tag{10}$$

Additionally, the following dimensionless quantities are defined:

$$\begin{aligned} &\beta = \frac{M}{m+M};\;\; u = \left(\frac{M}{EI}\right)^{1/2} UL;\;\; \gamma = \frac{(m+M)gL^3}{EI}; \\ &\kappa_0 = \frac{M_T L}{GI_p};\;\; \kappa_1 = \frac{EI_p}{EI};\;\; \kappa_2 = \frac{EAL^2}{EI};\;\; \kappa_3 = \frac{GI_p}{EI};\;\; \kappa_4 = \frac{EI_4}{EIL^2};\;\; \kappa_5 = \frac{J_p}{(m+M)L^2}. \end{aligned} \tag{11}$$

Using the notation $(\,)' = \partial(\,)/\partial\hat{s}$, where $\hat{s} = s/L$, and $\dot{(\,)} = \partial(\,)/\partial\tau$, the dimensionless equations of motion are determined as

$$\ddot{\xi} - \kappa_2\left[\xi'' + \frac{1}{2}\left(\eta'^2 + \zeta'^2\right)'\right] - \sqrt{\beta}u\left[\eta'\dot{\eta}' + \zeta'\dot{\zeta}' + \left(\eta'\dot{\eta} + \zeta'\dot{\zeta}\right)'\right] - \kappa_1\left[\theta_x'\theta_x'' - (\theta_x'\eta'\zeta'')'\right] + \\ + 2\left(\eta''\eta''' + \zeta''\zeta'''\right) - \left(\eta''\eta' + \zeta''\zeta' - \theta_x\eta''\zeta' + \theta_x\zeta''\eta'\right)'' - \gamma = 0, \tag{12}$$

governing the axial displacements $\xi$,

$$\ddot{\eta} + \eta'''' + \sqrt{\beta}u\left[2\dot{\eta}' - \dot{\xi}'\eta' - \xi'\dot{\eta}' - \frac{3}{2}\eta'^2\dot{\eta}' - \frac{1}{2}\dot{\eta}'\zeta'^2 - \eta'\zeta'\dot{\zeta}' - \left(\dot{\xi}\eta' + \xi'\dot{\eta} + \frac{3}{2}\eta'^2\dot{\eta} + \frac{1}{2}\dot{\eta}\zeta'^2 + \dot{\zeta}\zeta'\eta'\right)'\right] - \\ -\kappa_5\left(\dot{\theta}_x\dot{\zeta}' - \eta'\dot{\zeta}'^2\right)' - \kappa_2\left[\xi'\eta' + \frac{1}{2}\left(\eta'^2 + \zeta'^2\right)\eta'\right]' + \kappa_3\left(\theta_x'\zeta'' - \zeta''^2\eta'\right)' + \left(\xi''\eta'' - \frac{1}{2}\kappa_1{\theta_x'}^2\eta' + \eta'\zeta''^2 + \right. \\ \left. + 2\eta''^2\eta' + \eta''\zeta'\zeta''\right)' - \left(2\xi'\eta'' + \xi''\eta' + \eta''\zeta'^2 + 2\eta'^2\eta'' + \eta'\zeta'\zeta''\right)'' = 0, \tag{13}$$

governing the transverse displacements $\eta$,

$$\ddot{\zeta} + \zeta'''' + \sqrt{\beta}u\left[2\dot{\zeta}' - \dot{\xi}'\zeta' - \xi'\dot{\zeta}' - \eta'\dot{\eta}'\zeta' - \frac{1}{2}\eta'^2\dot{\zeta}' - \frac{3}{2}\zeta'^2\dot{\zeta}' - \left(\dot{\xi}\zeta' + \xi'\dot{\zeta} + \dot{\eta}\eta'\zeta' + \frac{1}{2}\eta'^2\dot{\zeta} + \frac{3}{2}\zeta'^2\dot{\zeta}\right)'\right] + \\ +\kappa_5\left(\ddot{\theta}_x\eta' + \dot{\theta}_x\dot{\eta}' - \ddot{\zeta}'\eta'^2 - 2\dot{\zeta}'\eta'\dot{\eta}'\right)' - \kappa_2\left[\xi'\zeta' + \frac{1}{2}\left(\eta'^2 + \zeta'^2\right)\zeta'\right]' - \kappa_3\left(\theta_x'\eta' - \eta'^2\zeta''\right)'' + \\ + \left(\xi''\zeta'' - \frac{1}{2}\kappa_1{\theta_x'}^2\zeta' + 2\zeta'\zeta''^2 + \zeta'\eta''^2 + \eta'\eta''\zeta''\right)' - \left(\xi''\zeta' + 2\xi'\zeta'' + 2\zeta'^2\zeta'' + \zeta''\eta'^2 + \eta''\eta'\zeta'\right)'' = 0, \tag{14}$$

governing the transverse displacements $\zeta$, and

$$\kappa_5\ddot{\theta_x} - \kappa_3\left[\theta_x'' - (\eta'\zeta'')'\right] - \kappa_5\left(\dot{\eta}'\dot{\zeta}' + \eta'\ddot{\zeta}'\right) - \kappa_1\left[\xi'\theta_x' + \frac{1}{2}\left(\eta'^2 + \zeta'^2\right)\theta_x'\right]' - \frac{1}{2}\kappa_4\left({\theta_x'}^3\right)' = 0. \tag{15}$$

governing the torsional displacements $\theta_x$.

Using the notation $(\,)_1 = (\,)(\hat{s} = 1)$, the generalized Hamilton's principle also provides the following natural boundary conditions:

$$\kappa_2\xi_1' + \sqrt{\beta}u\left(\dot{\xi}_1 + \eta_1'\dot{\eta}_1 + \zeta_1'\dot{\zeta}_1\right) + \frac{1}{2}\kappa_2\left({\eta_1'}^2 + {\zeta_1'}^2\right) + \kappa_1\left(\frac{1}{2}{\theta_{x,1}'}^2 - \theta_{x,1}'\zeta_1''\eta_1'\right) - \zeta_1''^2 - \eta_1''^2 + \\ + \left(\zeta_1''\zeta_1' + \eta_1''\eta_1' - \theta_{x,1}\eta_1''\zeta_1' + \theta_{x,1}\zeta_1''\eta_1'\right)' - \frac{u^2}{2}\left({\eta_1'}^2 + {\zeta_1'}^2\right) + u^2 = 0, \tag{16}$$

$$\kappa_2\left[\xi_1'\eta_1' + \frac{1}{2}\left({\eta_1'}^2 + {\zeta_1'}^2\right)\eta_1'\right] - \eta_1''' + \sqrt{\beta}u\left(\dot{\xi}_1\eta_1' + \xi_1'\dot{\eta}_1 + \frac{3}{2}{\eta_1'}^2\dot{\eta}_1 + \frac{1}{2}\dot{\eta}_1{\zeta_1'}^2 + \dot{\zeta}_1\zeta_1'\eta_1'\right) + \\ +\kappa_5\left(\dot{\theta}_{x,1}\dot{\zeta}_1' - \eta_1'\dot{\zeta}_1'^2\right) + \kappa_3\left(-\theta_{x,1}'\zeta_1'' + \eta_1'\zeta_1''^2\right) + \frac{\kappa_1}{2}{\theta_{x,1}'}^2\eta_1' - \xi_1''\eta_1'' - \eta_1'\zeta_1''^2 - 2\eta_1''^2\eta_1' - \\ -\zeta_1'\zeta_1''\eta_1'' + \left(2\xi_1'\eta_1'' + \xi_1''\eta_1' + \eta_1''{\zeta_1'}^2 + 2{\eta_1'}^2\eta_1'' + \eta_1'\zeta_1'\zeta_1''\right)' - u^2\left(\xi_1'\eta_1' + \frac{1}{2}{\eta_1'}^3 + \frac{1}{2}\eta_1'{\zeta_1'}^2 - \eta_1'\right) = 0, \tag{17}$$

$$\eta_1'' - 2\xi_1'\eta_1'' - \xi_1''\eta_1' - \eta_1''{\zeta_1'}^2 - 2{\eta_1'}^2\eta_1'' - \eta_1'\zeta_1'\zeta_1'' = 0, \tag{18}$$

$$\kappa_2\left[\xi_1'\zeta_1' + \frac{1}{2}\left({\eta_1'}^2 + {\zeta_1'}^2\right)\zeta_1'\right] - \zeta_1''' + \sqrt{\beta}u\left(\dot{\xi}_1\zeta_1' + \xi_1'\dot{\zeta}_1 + \dot{\eta}_1\eta_1'\zeta_1' + \frac{1}{2}{\eta_1'}^2\dot{\zeta}_1 + \frac{3}{2}{\zeta_1'}^2\dot{\zeta}_1\right) -$$
$$-\kappa_5\left(\ddot{\theta}_{x,1}\eta_1' + \dot{\theta}_{x,1}\dot{\eta}_1' - \ddot{\zeta}_1'{\eta_1'}^2 - 2\dot{\zeta}_1'\eta_1'\dot{\eta}_1'\right) + \kappa_3\left(\theta_{x,1}'\eta_1' - {\eta_1'}^2\zeta_1''\right)' + \frac{\kappa_1}{2}{\theta_{x,1}'}^2\zeta_1' -$$
$$-\left(\xi_1''\zeta_1'' + 2\zeta_1'\zeta_1''^2 + \eta_1''^2\zeta_1' + \eta_1'\eta_1''\zeta_1''\right) + \left(\xi_1''\zeta_1' + 2\xi_1'\zeta_1'' + 2{\zeta_1'}^2\zeta_1'' + \zeta_1''{\eta_1'}^2 + \eta_1''\eta_1'\zeta_1'\right)' -$$
$$-u^2\left(\xi_1'\zeta_1' + \frac{1}{2}{\eta_1'}^2\zeta_1' + \frac{1}{2}{\zeta_1'}^3 - \zeta_1'\right) = 0, \tag{19}$$

$$\zeta_1'' - \xi_1''\zeta_1' - 2\xi_1'\zeta_1'' - \kappa_3\left(\theta_{x,1}'\eta_1' - {\eta_1'}^2\zeta_1''\right) - 2\xi_1'\zeta_1'' - 2{\zeta_1'}^2\zeta_1'' - \eta_1''\eta_1'\zeta_1' - \zeta_1''{\eta_1'}^2 = 0, \tag{20}$$

and

$$\kappa_3\left(\theta_{x,1}' - \eta_1'\zeta_1''\right) + \kappa_1\left[\xi_1'\theta_{x,1}' + \frac{1}{2}\left({\eta_1'}^2 + {\zeta_1'}^2\right)\theta_{x,1}'\right] + \frac{1}{2}\kappa_4{\theta_{x,1}'}^3 - \kappa_0\kappa_3 = 0. \tag{21}$$

A noteworthy observation is that, due to the use of Euler angles to describe the kinematics of the system, several mathematical asymmetries can be seen in Eqs. (12-21).

## 3. METHODOLOGY

Due to the presence of gravity and internal flow, the axial displacements $\xi$ can be separated into static and dynamic parts. Analogously, due to the presence of a torsional moment applied at the free end of the pipe, the same applies to the torsional displacements $\theta_x$. Accordingly, the dynamics is formulated around these static solutions, i.e.

$$\xi = \xi_s + \xi_d \text{ and } \theta_x = \theta_{x,s} + \theta_{x,d}. \tag{22}$$

The static solutions are obtained by negleting time-dependent terms in Eqs. (12-21). The resultant ordinary differential equations (ODEs) are discretized using Galerkin's method, i.e.

$$\xi_s(\hat{s}) = \sum_{n=1}^{N_{as}} A_{s,n}(\tau)\phi_{s,n}(\hat{s}) \text{ and } \quad \theta_{x,s}(\hat{s}) = \sum_{n=1}^{N_{rs}} D_{s,n}(\tau)\Theta_{s,n}(\hat{s}), \tag{23}$$

where $\phi_{s,n} = \hat{s}^n$, for $n = 1, ..., N_{as}$, and $\Theta_{s,n} = \hat{s}^n$, for $n = 1, ..., N_{rs}$. This procedure leads to a set of nonlinear algebraic equations which are solved numerically using the fsolve function of Matlab®. The evaluated static solutions for the nonlinear system are an input to the subsequent dynamical analysis.

The time-dependent displacements are also approximated using Galerkin's method:

$$\xi_d(\hat{s},\tau) = \sum_{n=1}^{N_a} A_n(\tau)\phi_n(\hat{s}); \quad \eta(\hat{s},\tau) = \sum_{n=1}^{N_t} B_n(\tau)\psi_n(\hat{s});$$
$$\zeta(\hat{s},\tau) = \sum_{n=1}^{N_t} C_n(\tau)\psi_n(\hat{s}); \quad \theta_{x,d}(\hat{s},\tau) = \sum_{n=1}^{N_r} D_n(\tau)\Theta_n(\hat{s}). \tag{24}$$

where $\phi_n$, for $n = 1, ..., (N_a - 1)$, $\psi_n$, for $n = 1, ..., N_t$, and $\Theta_n$, for $n = 1, ..., (N_r - 1)$, are the correspondent modal shapes of the linearized problems (Blevins (1979)). The last shape functions for $\xi_d$ and $\theta_{x,d}$ are such that the initial axial and torsional strain energies are not exceedingly high. More specifically, the last shape function used in discretizing $\xi_d$ is always the one corresponding to the inextensibility condition (see Wadham-Gagnon *et al.* (2006)) while the last shape function for $\theta_{x,d}$, the one corresponding to the condition of zero torsional angles (see Eq. (7)), i.e.

$$\phi_{N_a}(\hat{s}) = \int_0^{\hat{s}}\left(-\frac{\eta(\hat{s},\tau=0)'^2}{2} - \frac{\zeta(\hat{s},\tau=0)'^2}{2}\right)d\hat{s}, \text{ and } \quad \Theta_{N_r}(\hat{s}) = \int_0^{\hat{s}}\eta(\hat{s},\tau=0)'\zeta(\hat{s},\tau=0)''d\hat{s}. \tag{25}$$

All stability analyses presented in Sec. 4 are made using the Lyapunov's indirect method. However, one notable difference between the classical Lyapunov's indirect method and the analyses herein carried out is that the occurrence of divergence and flutter are numerically sought after separately. Unless otherwise specified, the parameters kept fixed along Sec. 4 are $\gamma = 0$, $\kappa_1 = 2$, $\kappa_3 = 0.7$, $\kappa_4 = 0.1$, $\kappa_5 = 0.001$, $N_{as} = N_{rs} = 4$, $N_a = 3$, $N_r = 4$ and $N_t = 8$. The parameter $\kappa_2$ is set to 10000 in order to impose a near-inextensibility behavior to the pipe conveying fluid and thus most of the axial dynamical displacements seen are due to the occurrence of the transverse and torsional ones. Across all dynamical simulations, the only nontrivial initial condition given is $B_1 = 0.001$. Finally, every numerical integration is made using the ode45 function of Matlab®.

Before presenting the next section, which focuses mostly on the effects induced by a localized torsional moment in the stability and dynamics of the pipe, two results are shown. The first one serves as a benchmark for the present model and is a comparison between the critical flow velocity for a horizontal pipe obtained from the present model (with $\kappa_0 = 0$) and the one obtained using the model of an inextensible pipe published in (Gregory and Païdoussis, 1966a) (see Fig. 3(a)). Given that the extensibility is inherent in the present mathematical model, some differences can be noted, even with a large value of the axial stiffness dimensionless parameter $\kappa_2$. It is well documented in the literature that, for horizontal pipes, the critical flow velocity $u_c$ increases with an increase in the mass-ratio parameter $\beta$. As shown in Fig. 3(a), the difference between the extensible and inextensible model increases as $\beta$ increases and, similarly as reported in (Ghayesh *et al.*, 2013), it is always higher for extensible pipes.

Lastly, the effects of considering nonlinearities in the axial and torsional solutions are briefly discussed. This is made by comparing the numerical static solutions of the nonlinear problem to the analytical ones from the linearized problem, which can be easily obtained as

$$\xi_s = -\frac{\gamma}{2\kappa_2}\hat{s}^2 + \frac{(\gamma - u^2)}{\kappa_2}\hat{s} \text{ and } \theta_{x,s} = \kappa_0 \hat{s}. \tag{26}$$

For the case in which $\gamma = 25$, $u = 20$ and $\kappa_0 = 2\pi$, Fig. 3(b) shows that the effects of the nonlinearities in the static solutions can be noticeable. Firstly, the reader notices that the presence of torsional displacements imply in larger negative axial displacements when compared to the linear (and thus $\xi_s$ and $\theta_{x,s}$ are decoupled) case. On the other hand, the presence of a compressive force due to the discharging fluid lowers the torsional stiffness of the pipe, leading to higher torsional displacements for the nonlinear problem.

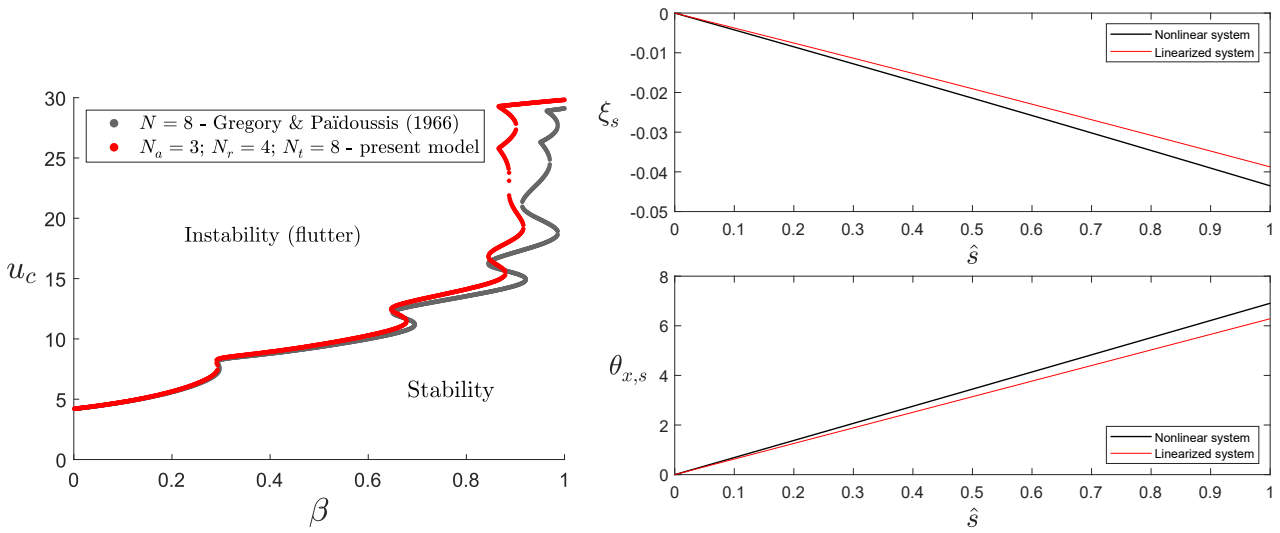


(a) (b)

Figure 3. (a) Comparison between the critical flow velocities for a horizontal pipe – present model and the one published in Gregory and Païdoussis (1966a) (inextensible); (b) Comparison between the axial and torsional static solutions of the nonlinear problem and those of the linearized problem for the case in which $\gamma = 25$, $u = 20$ and $\kappa_0 = 2\pi$.

## 4. RESULTS

This section aims to characterize the effects of a torsional moment applied at the free end of the pipe on its stability and post-critical dynamical behavior. More specifically, the critical flow velocities as a function of $\beta$ are compared between systems with ($\kappa_0 \neq 0$) and without ($\kappa_0 = 0$) the applied torsional moment.

It has been reported in the literature that the straight equilibrium configuration of beams may become unstable (divergence) when applied torsional moments are above a certain value (in the case of a simply supported beam, the reader is referred to (Greenhill, 1883)). In the present model, considering a horizontal pipe ($\gamma = 0$) with no internal flow, divergence is seen to occur when $\kappa_0 > \kappa_{0,c} \approx 0.76\pi$.

Consider first Fig. 4(a), which shows the critical flow velocities as a function of $\beta$ when a torsional moment of $\kappa_0 = 3\pi/4 < \kappa_{0,c}$ is applied at the free end of the pipe (red curve, online). Also shown in Fig. 4(a) are the critical flow velocities for the system without the addition of the torsional moment (grey curve, online).

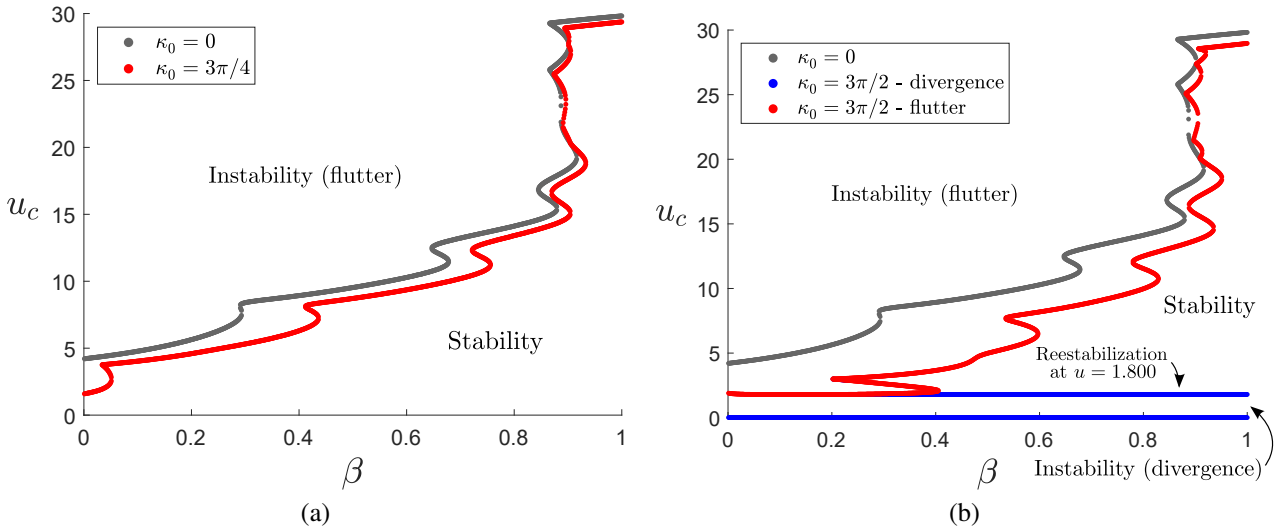


Figure 4. Critical flow velocities for a horizontal pipe with a torsional moment of magnitude (a) $\kappa_0 = 3\pi/4 < \kappa_{0,c}$ and (b) $\kappa_0 = 3\pi/2 > \kappa_{0,c}$ applied at its free end (red curve, online). The critical flow velocities for the system without the addition of a torsional moment is also shown (grey curve, online).

Firstly, no divergence is seen due to the fact that the value of the torsional moment is below its critical value, and the stability of the straight equilibrium configuration is qualitatively similar as when no torsional moments are applied. Thus, when the flow rate is above its critical value, flutter is seen to occur in both cases. However, quantitatively, Fig. 4(a) shows that the presence of a torsional moment implies on a reduction of the critical flow velocities across all values of $\beta$. Indeed, this reduction is relatively larger when very low values of $\beta$ are considered. Thus, for cases in which the conveyed fluid is air ($\beta \cong 0.001$ - (Gregory and Païdoussis, 1966b)) the presence of a torsional moment may severely reduce the flow rate above which flutter is seen to occur.

Figure 4(b) presents the same analysis when a torsional moment of $\kappa_0 = 3\pi/2 > \kappa_{0,c}$ is applied at the free end of the pipe. Now, since the value for $\kappa_0$ is above its critical value, the straight equilibrium configuration is unstable when $u = 0$. Depending on the value of $\beta$, two scenarios are seen to occur as the flow velocity is increased. When $\beta < 0.23$, increasing the flow velocity leads to flutter when it is above its critical value. When $\beta > 0.23$, however, the straight equilibrium configuration of the pipe becomes stable when the flow velocity surpasses $1.80$. If the flow rate is further increased and surpasses its critical value, which is now lower than when $\kappa_0 = 0$ or $\kappa_0 = 3\pi/4$, flutter takes place.

The two scenarios described above can also be observed when inspecting the root loci of the lowest-frequency vibrational modes of the system. Consider first the root loci presented in Fig. 5(a), in which $\kappa_0 = 3\pi/2 > \kappa_{0,c}$ and $\beta = 0.1$. As the flow velocity is increased from $0$ to $1.75$, the maximum $\Re(\lambda)$ decreases, albeit still comprised of positive values. When the flow velocity is between $1.75$ and $1.80$, the system is both subject to divergence and flutter. If $u$ is further increased, then it becomes only subject to flutter.

The root loci presented in Fig. 5(b), in turn, represents the scenario in which $\kappa_0 = 3\pi/2 > \kappa_{0,c}$ and $\beta = 0.7$. As $u$ is increased from $0$ to $1.80$, the maximum $\Re(\lambda)$ decreases and, if $1.80 < u < 8.92$, all eigenvalues possess a negative real part, i.e. the straight equilibrium configuration is stable. When $u > 8.92$, however, dynamic instability occurs. Therefore, divergence and flutter are not seen to coexist in this case.

The reader notices the qualitative similarity of the scenarios described above to when standing discharging pipes are considered, as discussed in Sec. 1. More specifically, when dealing with divergence due to an applied torsional moment or due to the compressive load of its own weight, the system can be capable of being “stabilized by flow”, as the author

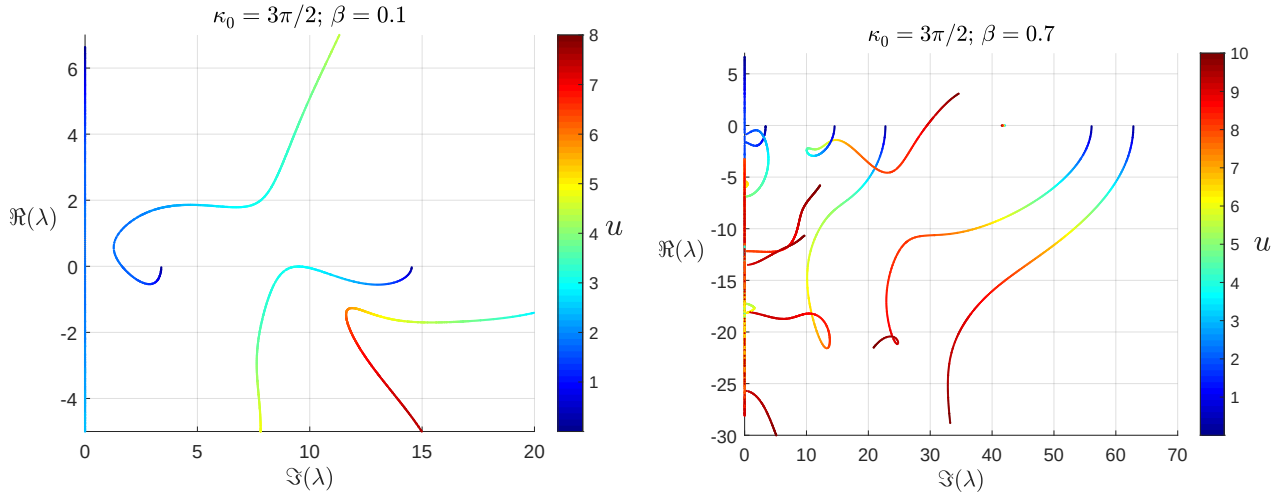


Figure 5. Root loci of the lowest-frequency modes of the system when $\kappa_0 = 3\pi/2 > \kappa_{0,c}$, (a) $\beta = 0.1$ and (b) $\beta = 0.7$.

in (Païdoussis, 1970) referred to this phenomenon. However, depending on the parameters characterizing the pipe, flutter may occur while the system is still subject to divergence.

The final results shown in this section are obtained by numerically integrating the equations of motion (Eqs. (12-15)) and natural boundary conditions (Eqs. (16-21)) of the mathematical model. All time series shown are for the free end of the pipe and represent different points shown in the root loci presented in Fig. 5(b), each with a different value of internal flow velocity.

First, consider Fig. 6, in which $u = 0.5$, and thus the system is subject only to divergence due to the addition of a torsional moment above its critical value. As expected, the pipe moves away from the unstable straight equilibrium configuration and, due to the internal-flow-induced damping, rests in the new equilibrium configuration in the steady state regime. Notice that the new equilibrium configuration does not remain in the $(x, z)$-plane, despite the fact that the initial configuration given does belong to it. In Fig. 7, on the other hand, a flow velocity of $u = 5$ is used. This value is high enough to inhibit the occurrence of divergence, but not enough to induce flutter. As expected, again due to the internal-flow-induced damping, the system rests in the steady state regime, but now in its stable straight equilibrium configuration.

The final set of time series is obtained using $u = 10 > u_c$ (Fig. 8), a value high enough to induce the occurrence of flutter. Under these conditions, the dynamics of the system resembles the classical limit-cycle oscillations exhibited by pipes when conveying fluid at post-critical flow velocities where, after an initial transient period, an oscillatory steady state regime is achieved. Interestingly, even though the initial conditions given are 2-D, the motions are 3-D due to the nonlinear coupling related to the applied torsional moment.

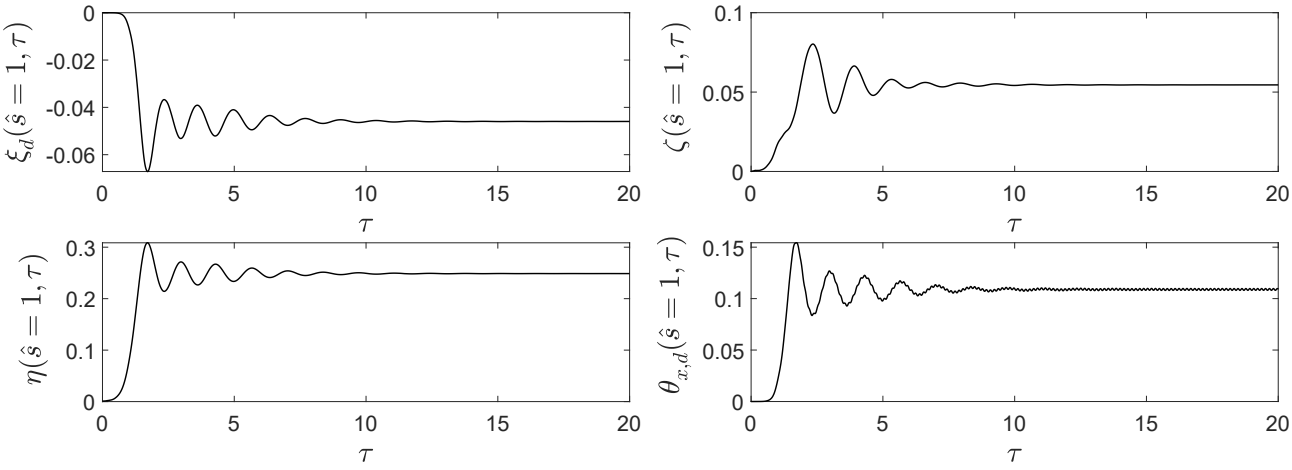


Figure 6. Time series obtained by numerically integrating the equations of motion (Eqs. (12-15)) and natural boundary conditions (Eqs. (16-21)) of the mathematical model using $u = 0.5 < u_c$.

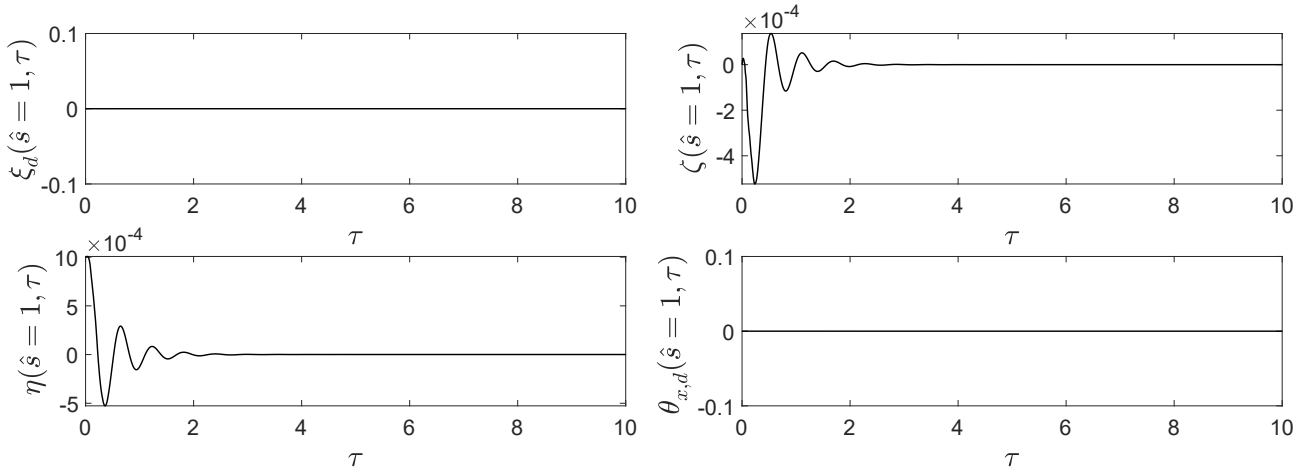


Figure 7. Time series obtained by numerically integrating the equations of motion (Eqs. (12-15)) and natural boundary conditions (Eqs. (16-21)) of the mathematical model using $u = 5 < u_c$.

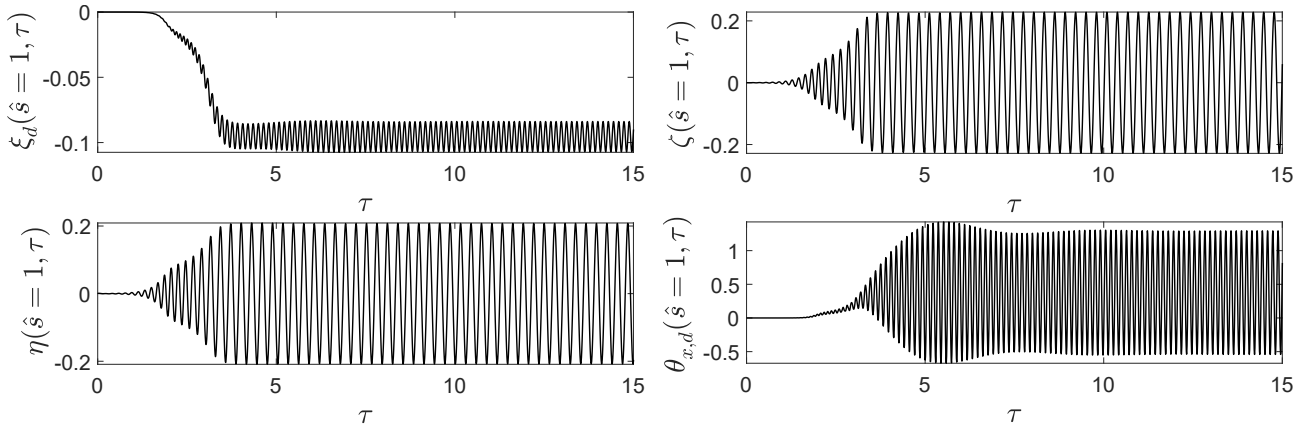


Figure 8. Time series obtained by numerically integrating the equations of motion (Eqs. (12-15)) and natural boundary conditions (Eqs. (16-21)) of the mathematical model using $u = 10 > u_c$.

## 5. CONCLUSIONS

In the present work, a 3-D nonlinear mathematical model for a cantilevered pipe conveying fluid was presented. The axial and torsional displacements were also considered in the dynamics and the nonlinearities were expanded up to the cubic order. The dynamics of the system was formulated around the axial and torsional static solutions which were numerically evaluated while considering the nonlinear static terms. Both the static and dynamical equations were discretized using Galerkin's method, albeit using different sets of shape functions. As a preliminary investigation of the role of torsion in the dynamics and stability of pipes conveying fluid, a torsional moment applied at the free end was included in the model. For the pipe filled with a still fluid, increasing the torsional moment above a critical value led to the straight equilibrium configuration losing stability due to divergence. For pipes characterized by higher values of the mass-ratio parameter $\beta$, a stabilization by internal flow was seen possible, and divergence and flutter were not observed. For lower values of $\beta$, in turn, divergence and flutter may occur for a narrow range of internal flow velocities. For pipes with sub-critical torsional moments applied at its free end, it was shown that the critical flow velocities are always lower than for pipes without applied torsional moments. By numerically integrating the mathematical model in different scenarios, a preliminary characterization of the effects of the applied torsional moment in the nonlinear dynamics of the pipe was addressed. It was shown that the motion of the pipe with the application of the torsional moment was 3-D even when 2-D initial conditions were given. In such scenarios, the motion of the pipe is always 2-D if no torsional moment is applied at its free end. The work herein presented will be further developed to include other placement positions for the torsional moment. More detailed investigations of the role of torsion in the nonlinear dynamics of pipes conveying fluid are also planned to be developed.

## ACKNOWLEDGEMENTS

The first author aknowledges the São Paulo Research Foundation (FAPESP) for his PhD scholarship (grant 2021/04434-1) and for the research internship scholarship at Concordia University (grant 2022/12546-7). FAPESP is also acknowledged for the financial support to a Thematic Project on the applications of nonlinear dynamics to engineering systems (grant 2022/00770-0). The third author is grateful to Ministère des Relations internationales et de la Francophonie for providing a mobility funding under Projet de coopération Québec-Brésil as well as to the Natural Sciences and Engineering Research Council of Canada. The fourth author thanks the Brazilian Research Council for the grant 305945/2020-3.

## REFERENCES

Askarian, A. and Kheiri, M., 2018. "Three-dimensional nonlinear dynamics of an extensible pipe conveying fluid". In *9th International Symposium on Fluid-Structure Interactions, Flow-Sound Interactions, Flow-Induced Vibration & Noise*.

Benjamin, T.B., 1961. "Dynamics of a system of articulated pipes conveying fluid. I. Theory". *Proceedings of the Royal Society*, Vol. 261, pp. 457–486.

Blevins, R., 1979. *Formulas for natural frequency and mode shape*. Litton Educational Publishing.

Casetta, L. and Pesce, C.P., 2013. "The generalized Hamilton's principle for a non-material volume". *Acta Mechanica*, Vol. 224, pp. 919–924. doi:10.1007/s00707-012-0807-9.

Crespo da Silva, M.R.M., 1988. "Non-linear flexural-flexural-torsional-extensional dynamics of beams — I. Formulation". *International Journal of Solids and Structures*, Vol. 24, pp. 1225–1234. doi:https://doi.org/10.1016/0020-7683(88)90087-X.

Ghayesh, M.H., Païdoussis, M.P. and Amabili, M., 2013. "Nonlinear dynamics of cantilevered extensible pipes conveying fluid". *Journal of Sound and Vibration*, Vol. 332, pp. 6405–6418.

Greenhill, A.G., 1883. "On the strength of shafting when exposed both to torsion and to end thrust". *Proceedings of the Institution of Mechanical Engineers*, Vol. 34, No. 1, pp. 182–225.

Gregory, R.W. and Païdoussis, M.P., 1966a. "Unstable oscillation of tubular cantilevers conveying fluid. I. Theory". *Proceedings of the Royal Society*, Vol. 293, pp. 512–527.

Gregory, R.W. and Païdoussis, M.P., 1966b. "Unstable oscillation of tubular cantilevers conveying fluid. II. Experiments". *Proceedings of the Royal Society*, Vol. 293, pp. 528–542.

Irschik, H. and Holl, H.J., 2002. "The equations of Lagrange written for a non-material volume". *Acta Mechanica*, Vol. 153, pp. 231–248. ISSN 00015970. doi:10.1007/BF01177454.

Kheiri, M. and Païdoussis, M.P., 2014. "On the use of generalized Hamilton's principle for the derivation of the equation of motion of a pipe conveying fluid". *Journal of Fluids and Structures*, Vol. 50, pp. 18–24. ISSN 10958622. doi:10.1016/j.jfluidstructs.2014.06.007.

McIver, D.B., 1973. "Hamilton's principle for systems of changing mass". *Journal of Engineering Mathematics*, Vol. 7, pp. 249–261.

Païdoussis, M.P., 1970. "Dynamics of tubular cantilevers conveying fluid". *Journal of Mechanical Engineering Science*, Vol. 12, pp. 85–103. doi:10.1243/JMES.

Païdoussis, M.P., 2014. *Fluid-Structure Interactions: Slender Structures and Axial Flow*. Academic Press.

Païdoussis, M.P. and Li, G.X., 1992. "Pipes conveying fluid: A model dynamical problem". *Journal of Fluids and Structures*, Vol. 7, pp. 137–204. doi:10.1006/jfls.1993.1011.

Païdoussis, M.P., 2022. "Pipes conveying fluid: A fertile dynamics problem". *Journal of Fluids and Structures*, Vol. 114, p. 103664. ISSN 0889-9746. doi:https://doi.org/10.1016/j.jfluidstructs.2022.103664. URL `https://www.sciencedirect.com/science/article/pii/S0889974622000974`.

Semler, C., Li, G.X. and Païdoussis, M.P., 1992. "The non-linear equations of motion of pipes conveying fluid". *Journal of Sound and Vibration*, Vol. 169, pp. 577–599.

Wadham-Gagnon, M., Païdoussis, M.P. and Semler, C., 2006. "Dynamics of cantilevered pipes conveying fluid. Part 1: Nonlinear equations of three-dimensional motion". *Journal of Fluids and Structures*, Vol. 23, pp. 545–567.